Received: 15 February 2022 | Revised: 27 March 2022 | Accepted: 28 March 2022

DOI: 10.1002/htj.22540

ORIGINAL ARTICLE

HEAT TRANSFER WILEY

On transient MHD heat transfer within a radiative porous channel due to convective boundary conditions

Bala Yabo Isah[1] | **Bashiru Abdullahi**[2] | **Ibrahim Y. Seini**[3]

[1]Department of Mathematics, Usmanu Danfodiyo University Sokoto, Sokoto, Nigeria

[2]Department of Mathematics and Statistics, Abdu Gusau Polytechnic, Talata Mafara, Zamfara State, Nigeria

[3]Department of Mechanical Engineering, School of Engineering, University for Development Studies, Tamale, Ghana

Correspondence
Bashiru Abdullahi, Department of Mathematics and Statistics, Abdu Gusau Polytechnic, Talata Mafara PMB 1021, Zamfara State, Nigeria.
Email: malbashmaf@yahoo.com

Funding information
Tertiary Education Trust Fund

Abstract

In this paper, the steady/transient magnetohydrodynamics heat transfer within a radiative porous channel due to convective boundary conditions is considered. The solution of the steady-state and that of the transient version were conveyed by the perturbation and finite difference methods, respectively. The heat transfer mechanism of the present work ascertain the influence of Biot number (B_{i1}), magnetizing parameter (M), radiation parameter (R), temperature difference, suction/injection (S), Grashof number (Gr), and time (t) on velocity (u), temperature (θ), skin friction (τ), and Nusselt number (Nu). The results were established and discussed with the help of a line graph. It was found that the velocity, temperature, and skin friction decay with increasing suction/injection and magnetizing parameters while the Nusselt number upsurges with suction/injection at $y=0$ and falls at $y=1$. The steady-state solution was in perfect agreement with the transient version for a significant value of time *t*. It is interesting to report that the Biot number has a cogent influence consequently, as its values upsurge the result of the present work slant the extended literature.

KEYWORDS

convective boundary condition, heat transfer, MHD, porous channel, thermal radiation, transient

1 | INTRODUCTION

The scientific eruption has continuously brought about a great awakening in the field of heat transfer on magnetohydrodynamics (MHD) as the industrial revolution necessitates a good fraction of the social well-being of its society to the use of heat as a source of energy. As such, studies on porous (suction/injection) mediums have become a prominent theme of discussion in the area of MHD heat transfer. As a case in point, such as marine (thrust bearing) generators, radial (oil, fluorescent light, etc.) diffusers, heavy oil (thermal oil recovery) reservoirs, to mention but a few, suction/injection is applied to enhance and stabilize. Therefore, the quest for the relevant application of suction/injection on MHD heat transfer drives the efforts of many authors in conducting research on the related topic in recent years.[1–13]

A prodigious deal of interest in MHD fluids control by heat flux continues to flourish. For instance, a heat transfer system operating at high temperatures requires a reasonable amount of radiation. For example, Dulal and Babulal[14] reported that in the design (production and process industries) basic quality of thermal radiation is needed with excellent thermal stability. Considering the above application of thermal radiation in the field of engineering technology, many authors have shown interest in thermal MHD heat transfer.[7,9,15–19]

MHD prescribed by convective boundary conditions continues to play an important role in engineering and industrial (transpiration, cooling process, material drying, etc.) processes. Recently a handful of researchers have worked on MHD flow subject to convective boundary conditions.[20–24]

Considering the importance of convective boundary conditions in engineering and technology and also taking cognizance of fluids flow within channels are exposed to environments of different or changing temperatures, the present study is motivated to extend the work of Isah et al.[18] to incorporate the convective boundary conditions. The objective of the present work is aimed at solving the said problem both analytically and numerically using perturbation and unconditional finite different methods in view to address the efficacy of the convective (Biot number) parameter in the presence of pertinent parameters within a radiative porous channel.

2 | GOVERNING EQUATIONS

The geometry of Figure 1 reflects the flow configuration of steady/transient laminar (MHD) through porous walls guided by a magnetic field with intensity B_0. The x'-coordinate is taken in the direction of the main flow along with the plate and the y'-coordinate is normal to the plate. Earlier in the start-up of the experiment, the dimensional time is assumed to be $t' \leq 0$ such that the fluid and plate exhibit a constant temperature T_0. It is further assumed that the temperature of the wall situated at $y' = 0$, received a convection energy $-k^* \frac{\partial T'}{\partial y'}\Big|_{y'=0} = h_1\left[T_1 - T'\left(0, t\right)\right]$ while reference temperature at $y = H$ is maintained as T_0 at dimensional time $t' > 0$. Under Boussinesq approximation and presuming the flow to be laminar and fully developed, the dimensional form of velocity and temperature equations are given below:

$$\frac{\partial u'}{\partial t'} + V_0 \frac{\partial u'}{\partial y'} = \nu \frac{\partial^2 u'}{\partial y'^2} + g\beta(T_1 - T_0) - \sigma \frac{B_0^2 u'}{\rho}, \tag{1}$$

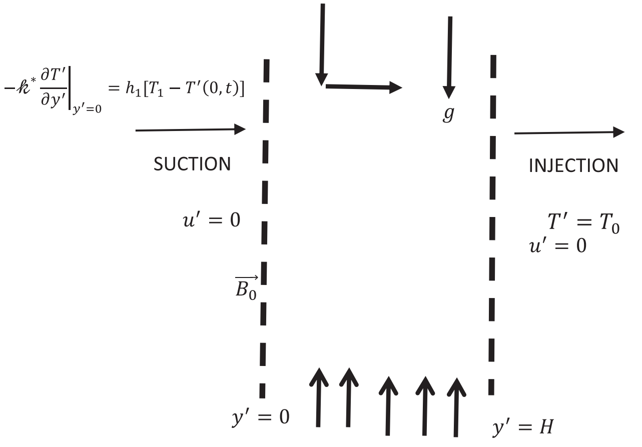

FIGURE 1 The geometry of the problem for the porous channel

$$\frac{\partial T'}{\partial t'} + V_0 \frac{\partial T'}{\partial y'} = \alpha \left[\frac{\partial^2 T'}{\partial y'^2} - \frac{1}{K} \frac{\partial q_y}{\partial y'} \right], \tag{2}$$

and the presumed initial/boundary conditions to be satisfied are given below:

$$\begin{aligned} &t' \le 0 : u' = 0;\ T' = T_0, && \text{for} \quad 0 \le y' \le H, \\ &t' > 0 : u' = 0,\ -k^* \frac{\partial T'}{\partial y'}\Big|_{y'=0} = h_1 \left[T_1 - T'\left(0, t\right) \right] && \text{at} \quad y' = 0, \\ &u' = 0,\ T' = T_0 && \text{at} \quad y' = H. \end{aligned} \tag{3}$$

The radiation heat flux (q_y) on the right-hand verge of (2) is in the y'-direction whereas its effect is measured as insignificant in the latter direction (x'). The current investigation is restricted to optically dense fluids[18]

$$q_y = \frac{-4\sigma^* \partial T'^4}{3k^* \partial y'}. \tag{4}$$

The dimensional quantities σ^* and k^* represent the Stefan–Boltzmann constant and the mean absorption constant, respectively. Conditioning the value of T'^4 significantly small, one can linearize Equation (4) such that;

$$T'^4 = (\theta(T_1 - T_0) + T_0)^4. \tag{5}$$

The follow-on dimensionless quantities are ascertained as:

$$\begin{aligned} &t = \frac{t'\nu}{H^2}, y = \frac{y'}{H}, P_r = \frac{\nu}{\alpha}, \theta = \frac{T' - T_0}{T_1 - T_0}, B_{i1} = \frac{h_1 H}{k^*}, G_r = \frac{[g\beta H^2 (T_1 - T_0)]}{\nu U}, \\ &M^2 = \frac{\sigma \beta_0^2 H^2}{\nu}, u = \frac{u'}{U}, R = \frac{4\sigma^* (T_1 - T_0)^3}{K k^*}, C_T = \frac{T_0}{T_1 - T_0}, S = \frac{V_0 H}{\nu}. \end{aligned} \tag{6}$$

As a result of Equation (6) in (1) and (2) subject to (3), the velocity and temperature equations are streamlined as follows;

$$\frac{\partial u}{\partial t} + S\frac{\partial u}{\partial y} = \frac{\partial^2 u}{\partial y^2} + Gr\theta - M^2 u, \tag{7}$$

$$P_r\left[\frac{\partial \theta}{\partial t} + S\frac{\partial \theta}{\partial y}\right] = \left[1 + \frac{4R}{3}(C_T + \theta)^3\right]\frac{\partial^2 \theta}{\partial y^2} + 4R[C_T + \theta]^2\left(\frac{\partial \theta}{\partial y}\right)^2, \tag{8}$$

and ease the initial and boundary conditions as:

$$\begin{cases} t \le 0 : u = 0, \theta = 0, & \text{for } \ 0 \le y \le 1. \\ t > 0 : u = 0, -\frac{d\theta}{dy}\Big|_{y=0} = B_{i1}[1 - \theta], & \text{at } \ y = 0. \\ u = 0, \theta = 0 & \text{at } \ y = 1. \end{cases} \tag{9}$$

3 | ANALYTICAL SOLUTION

Indeed the Rosseland approximation described in Equation (8) turns the present physical problem highly nonlinear and exhibits no closed-form solution. However, the resulting steady-state solution of MHD heat transfer within a radiative porous channel due to convective boundary conditions can be useful in validating the numerical result of the coupled nonlinear time of MHD heat transfer within a radiative porous channel due to convective boundary condition. Therefore the baseline Equations (7)–(9) can be visualized in steady form for velocity and temperature, respectively, as;

$$S\frac{du}{dy} = \frac{d^2 u}{dy^2} + Gr\theta - M^2 u. \tag{10}$$

$$P_r S\frac{d\theta}{dy} = \left[1 + \frac{4R}{3}(C_T + \theta)^3\right]\frac{d^2\theta}{dy^2} + 4R[C_T + \theta]^2\left(\frac{d\theta}{dy}\right)^2. \tag{11}$$

With the following boundary conditions:

$$\left.\begin{aligned} &\text{at } \ y = 0, \ \ u = 0, \frac{d\theta}{dy} = B_{i1}(1 + \theta). \\ &\text{at } \ y = 1, \ \ u = 0, \theta = 0. \end{aligned}\right\} \tag{12}$$

Implementing the regular perturbation ($R \ll 1$) method the velocity (u), and temperature (θ) are approximated as;

$$u(y) = \sum_{j=0}^{\infty} R^j u_j(y), \tag{13}$$

$$\theta(y) = \sum_{j=0}^{\infty} R^j \theta_j(y). \tag{14}$$

Switching Equations (13) and (14) into (10) and (11), respectively, and drooping the higher powers of $R > 1$ the required steady-state solution for $u(y)$ and $\theta(y)$ subject to boundary condition (12) reads:

$$u(y) = a_{23}e^{x_1 y} + a_{24}e^{x_2 y} + a_{25} + a_{26}e^{P_r S y} + R(G_{21}e^{x_3 y} + G_{22}e^{x_4 y} + G_{23} + G_{24}e^{P_r S y} + G_{25} ye^{P_r S y} + G_{26}e^{2P_r S y} + G_{27}e^{3P_r S y} + G_{28}e^{4P_r S y}). \tag{15}$$

$$\theta(y) = a_{21} + a_{22}e^{P_r S y} + R(d_{21} + d_{22}e^{P_r S y} + d_{23}ye^{P_r S y} + d_{24}e^{2P_r S y} + d_{25}e^{3P_r S y} + d_{26}e^{4P_r S y}). \tag{16}$$

The steady-state skin friction at the boundaries is:

$$\tau_0 = \left.\frac{du}{dy}\right|_{y=0} = a_{23}x_{21} + a_{24}x_{22} + a_{26}P_r S + Re_{21}x_{23} + Re_{22}x_{24} + Rk_{22}P_r S + Rk_{23} + 2Rk_{24}P_r S + 3Rk_{25}P_r S + 4Rk_{26}P_r S. \tag{17}$$

$$\tau_1 = \left.\frac{du}{dy}\right|_{y=1} = a_{23}x_{21}e^{x_{21}} + a_{24}x_{22}e^{x_{22}} + a_{26}P_r^{P_r S} + Re_{21}x_{23}e^{x_{23}} + Re_{22}x_{24}e^{x_{24}} + Rk_{22}P_r^{P_r S} + Rk_{23}P_r Se^{P_r S} + Rk_{23}e^{P_r S} + 2Rk_{24}P_r^{2P_r S} + 3Rk_{25}P_r Se^{3P_r S} + 4Rk_{26}P_r^{4P_r S}. \tag{18}$$

While the steady-state Nusselt number at the same boundaries becomes:

$$N_{u_0} = \left.\frac{d\theta}{dy}\right|_{y=0} = a_{22}P_r S + Rd_{22}P_r S + Rd_{23} + 2Rd_{24}P_r S + 3Rd_{25}P_r S + 4Rd_{26}P_r S. \tag{19}$$

$$N_{u_1} = \left.\frac{d\theta}{dy}\right|_{y=1} = a_{22}P_r Se^{P_r S} + Rd_{22}P_r^{P_r S} + Rd_{23}P_r Se^{P_r S} + Rd_{23}e^{P_r S} + 2Rd_{24}P_r^{2P_r S} + 3Rd_{25} P_r^{3P_r S} + 4Rd_{26}P_r Se^{4P_r S}. \tag{20}$$

4 | NUMERICAL EXPLANATION

As the mathematical prototype (7 and 8) capturing the present physical situation are coupled and highly nonlinear, the present work can be nicely solved via the unconditional (Implicit) finite difference method.

$$\frac{u_i^{j+1} - u_i^j}{\Delta t} + S\frac{u_{i+1}^j - u_{i-1}^j}{2\Delta y} = \left[\frac{u_{i-1}^{j+1} - 2u_i^{j+1} + u_{i+1}^{j+1}}{(\Delta y)^2}\right] - M^2u_i^j + Gr\theta_i^j, \tag{21}$$

$$P_r\left[\frac{\theta_i^{j+1} - \theta_i^j}{\Delta t} + S\frac{\theta_{i-1}^j - \theta_{i+1}^j}{2\Delta y}\right] = z_1\left[\frac{\theta_{i-1}^{j+1} - 2\theta_i^{j+1} + \theta_{i+1}^{j+1}}{(\Delta y)^2}\right] + z_2\left(\frac{\theta_{i-1}^j - \theta_{i+1}^j}{2\Delta y}\right)^2. \tag{22}$$

With boundary condition

$$\left\{\begin{array}{ll} u_i^j = 0, & \\ -\left[\dfrac{-3\theta_{i-1}^{j+1} + 4\theta_i^{j+1} - \theta_{i+1}^{j+1}}{2\Delta y}\right] = B_{i1}\left[1 - \theta_i^j\right], & \text{for all } i = 0. \\ -\left[\dfrac{-3\theta_{i-1}^{j+1} + 4\theta_i^{j+1} - \theta_{i+1}^{j+1}}{2\Delta y}\right] = B_{i1}\left[1 - \theta_i^j\right], & \\ u_M^j = 0, \theta_M^j = 0. & \end{array}\right\} \tag{23}$$

In summary, Equations (21)–(23) can be rewritten as;

$$B_l u_{i-1}^{j+1} + B_c u_i^{j+1} + B_r u_{i+1}^{j+1} = r_1 u_{i-1}^j - r_1 u_{i+1}^j + (1 - \Delta t M^2) u_i^j + \Delta t Gr \theta_i^j, \tag{24}$$

$$A_l \theta_{i-1}^{j+1} + A_c \theta_i^{j+1} + A_r \theta_{i+1}^{j+1} = Pr\theta_i^j + Prr_1 \theta_{i+1}^j - Prr_1 \theta_{i-1}^j + z_2 r_3 \left(\theta_{i-1}^j - \theta_{i+1}^j\right)^2. \tag{25}$$

AS the values of θ_0^j and θ_0^{j+1} at $y = 0$ are not defined from the boundary condition (23), one can modify Equation (25) using (23) for $i = 1$ to have;

$$\begin{aligned} \left(\frac{(4 - 2\Delta y B_{i1})}{3} A_l + A_c\right)\theta_1^{j+1} + \left(A_r - \frac{A_l}{3}\right)\theta_2^{j+1} + \frac{2}{3} A_l \Delta y B_{i1} = \left(Pr - \frac{(4 - 2\Delta y B_{i1})}{3} Prr_1\right) \\ \theta_1^j + \frac{4}{3} Prr_1 \theta_2^j - \frac{2}{3} Prr_1 \Delta y B_{i1} + z_2 r_3 \\ \left(\frac{(4 - 2\Delta y B_{i1})}{3}\theta_1^j - \frac{4}{3}\theta_2^j + \frac{2}{3}\Delta y B_{i1}\right)^2. \end{aligned} \tag{26}$$

The Scheme is convergent, unconditionally stable, and does not impose restriction $\left(\frac{\Delta t}{\Delta y^2}\right)$ mesh ratio, hence having the initial guess of θ at grid ($t = 0$) points, the system is reduced into a tridiagonal matrix and the temperature field ($t_{i+1} = t_i + \delta t$) obtained is a reference to the identified values of the preceding time $= t_i$ for all $i = 1, 2, \ldots M$. Hence, the acknowledged value of the temperature field obtained ($t_{i+1} = t_i + \delta t$) is used to evaluate velocity. This procedure is updated until the essential solutions (θ and u) are achieved at the merging benchmark:

$$|(u, \theta)_{\text{exact}} - (u, \theta)_{\text{num}}| < 10^{-4}. \tag{27}$$

5 | RESULT VALIDATION

Figure 2A,B show the comparison between the numerical solution (unsteady) and that of the analytical solution (steady-state). Under some limiting criteria, the two results were found to be in agreement at a large value of time. This clearly guarantees the robustness of our numerical scheme.

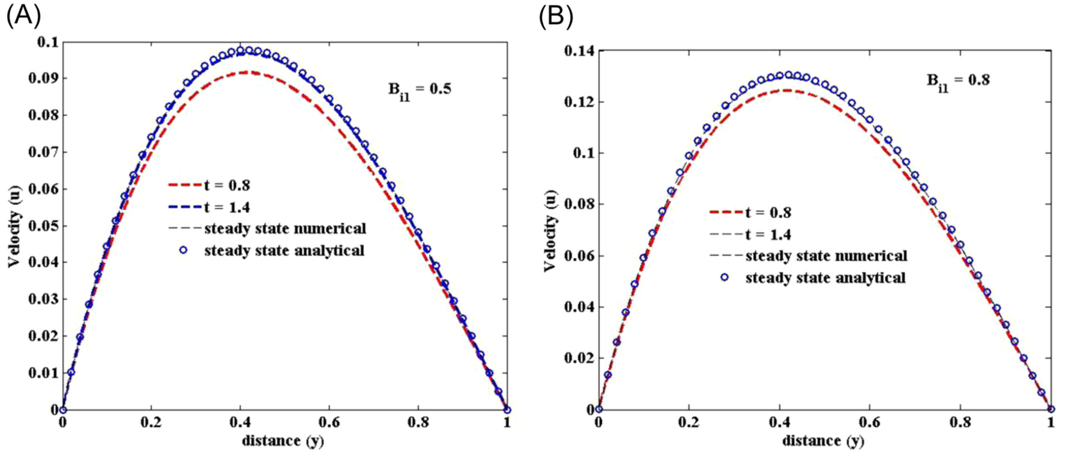

FIGURE 2 Upshot of steady/transient state velocity $u(y, t)$ outline

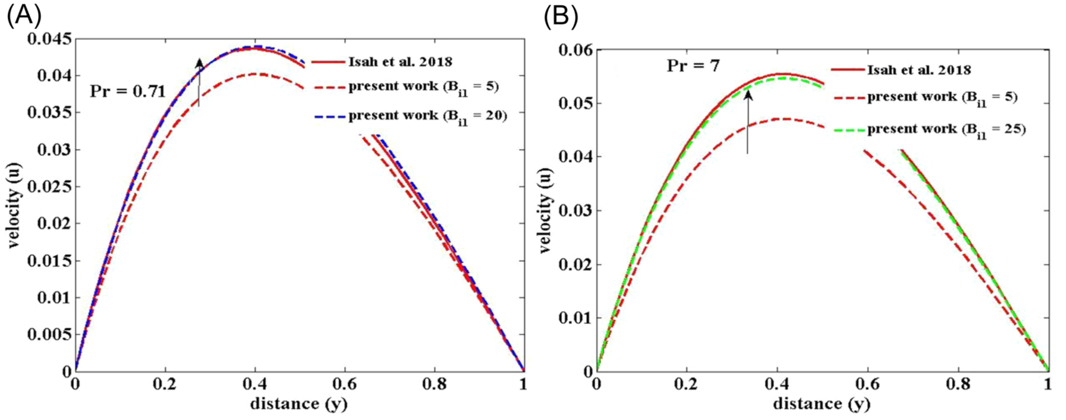

FIGURE 3 Upshot of convective boundary condition on velocity $u(y, t)$ outline

6 | RESULTS AND DISCUSSION

The result of steady and transient solution of MHD heat transfer is ascertained. The impact of the appropriate nondimensional flow parameters has been deliberated using line graphs as shown in Figures 2–19 in the form of velocity, temperature distribution, skin friction, and Nusselt number profiles. All the pertinent parameters are chosen arbitrary with the fixed default as $M = 1$, $R = 0.0001$, $C_T = 0.01$, $B_{i1} = 0.5$, $S = 0.1$, and $-0.5 \leq Gr \leq 5.0$ while the working fluid parameter (the Prandtl number) $Pr = 0.71$ and 7.0, which physically represent air and water, respectively.

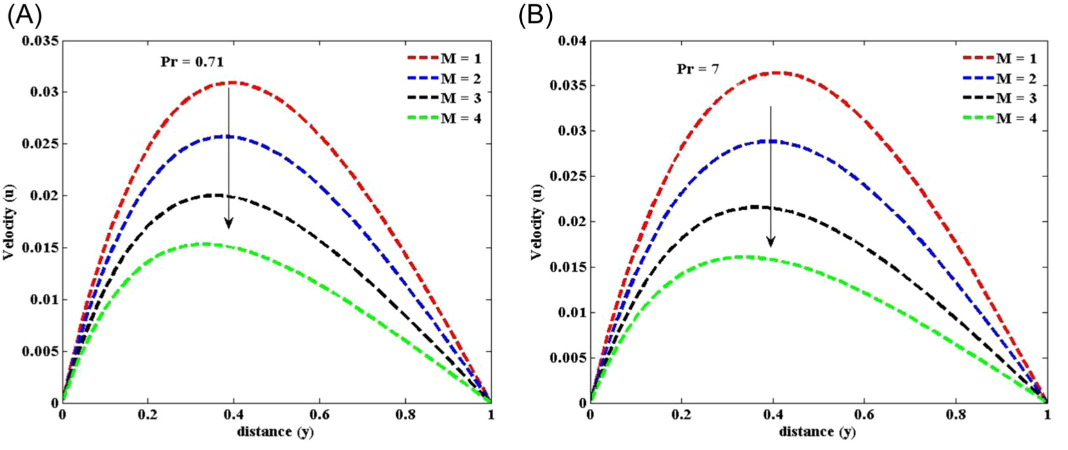

FIGURE 4 Upshot of M on velocity $u(y, t)$ outline

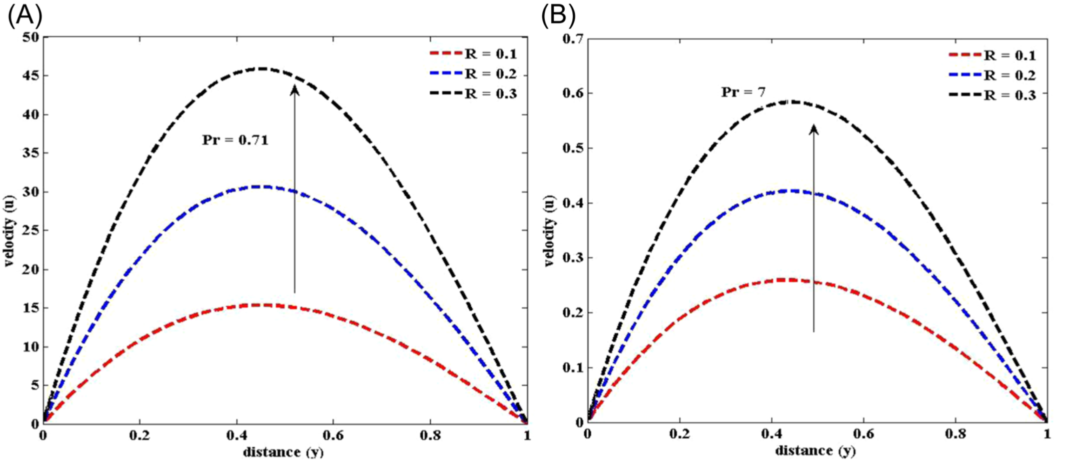

FIGURE 5 Upshot of R on velocity $u(y, t)$ outline

6.1 | Velocity profile

Figures 3–6 give highlights of velocity profiles due to pertinent parameters. The comparison between the present work and that of Isah et al.[18] is shown in Figure 3. Essentially, it is observed that the convective (Biot number) parameter boosts the values of velocity in the present work. This physically indicates that for the high value of the Biot number the internal heat resistance in the channel is high than the external resistance, hence it assists the velocity and can as well act as a stabilizer. Interestingly as the Biot number increases the result of the present work approaches that of Isah et al.[18] Figure 4A,B examines the retarding effect of the magnetic parameter (M) on the velocity outline. This physically reveals that as the magnetic field increases it expands the magnetic strength and it additionally upsurges the fluid particle, so velocity diminishes. Figure 5A,B represents the outcome effect of the radiation parameter.

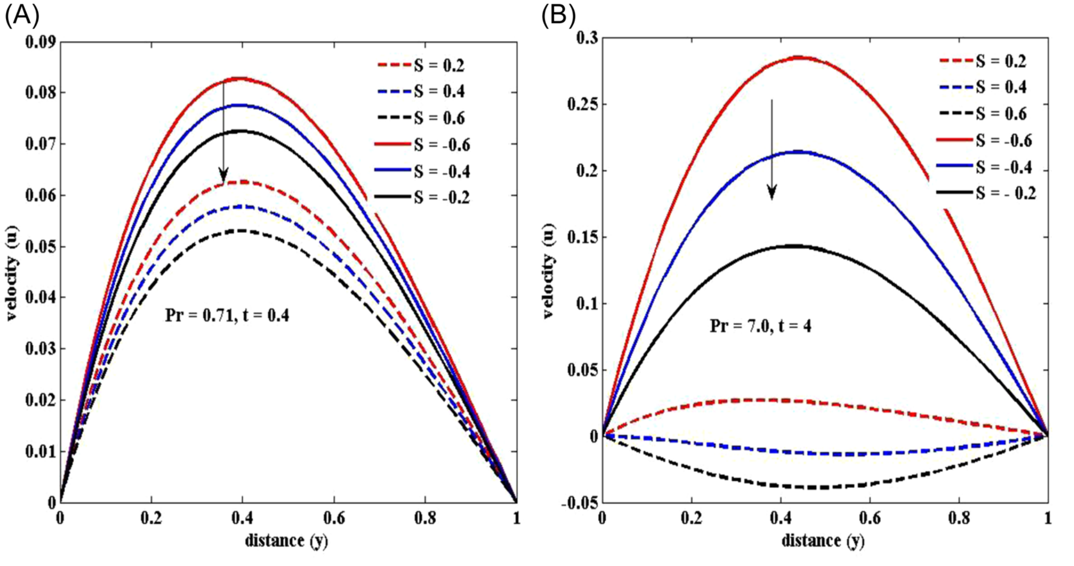

FIGURE 6 Upshot of S on velocity $u(y, t)$ outline

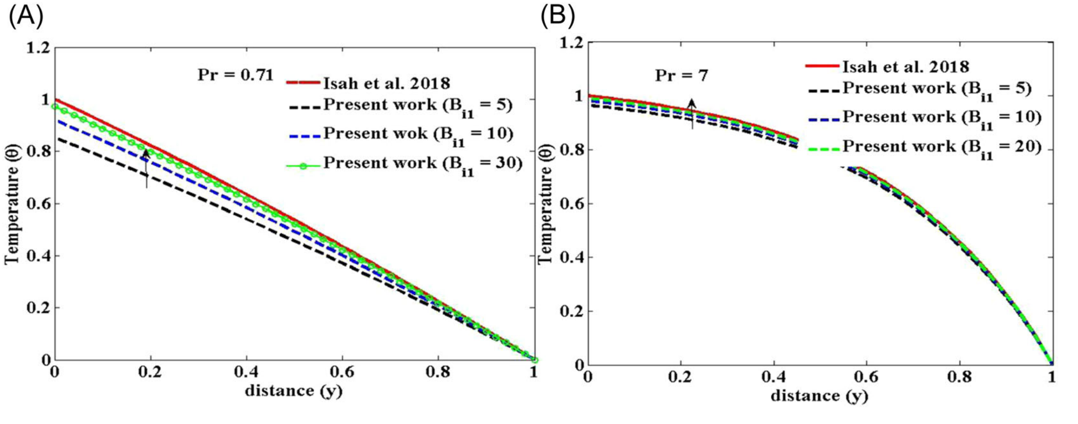

FIGURE 7 Upshot of convective boundary condition on temperature $\theta(y, t)$ outline

The velocity outlines improved, since thermal radiation accelerates the fluid velocity, through the boundary layer field. Figure 6A,B shows the influence of the suction/injection parameter (S) on the velocity outline. It is witnessed that the velocity of the fluid slows down due to suction ($S < 0$) and injection ($S > 0$) at $y = 0$ while it fast tracks in the case of suction in contrast with injection.

6.2 | Temperature profiles

Figures 7–10 indicate the effects of flow dimensionless parameters of the temperature outline. Figure 7A,B illustrates the present work temperature and that of Isah et al.[18] extended

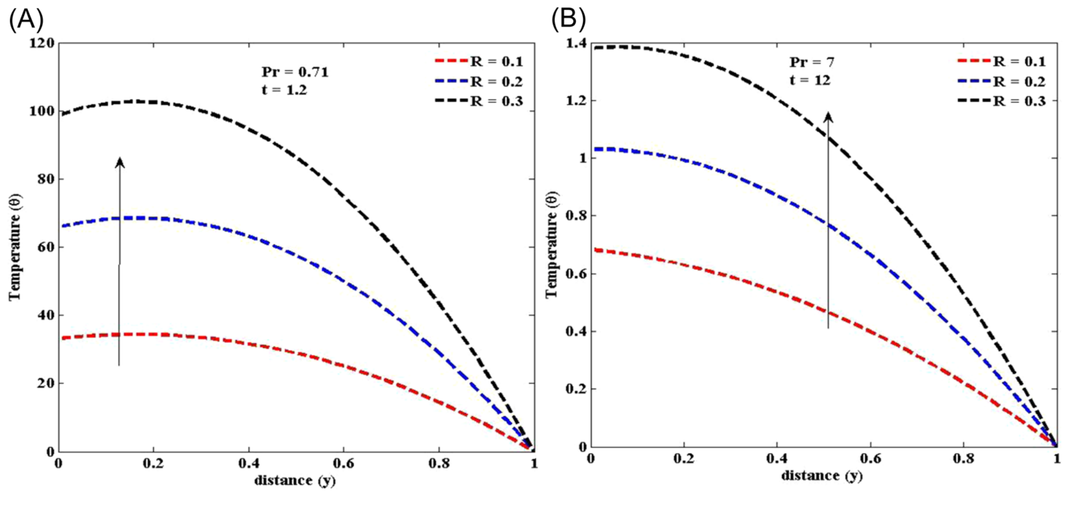

FIGURE 8 Upshot of R on temperature $\theta(y, t)$ outline

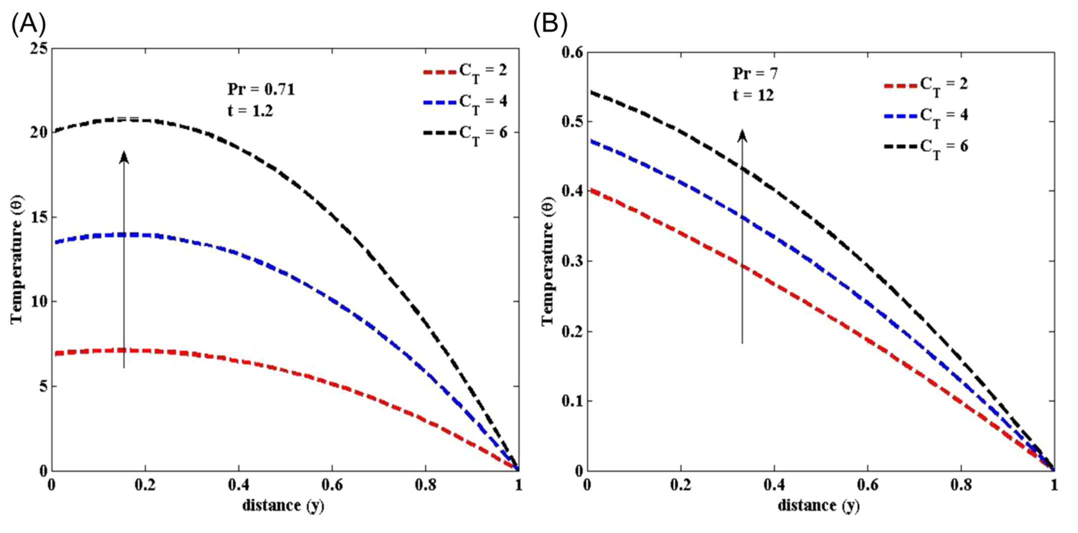

FIGURE 9 Upshot of C_T on temperature $\theta(y, t)$ outline

literature. It is observed that as the Biot number is growing bigger the temperature of the present is approaching that of Isah et al.[18] Figure 8A,B indicate the effect of radiation parameters on temperature outline. In Figure 8A, it is apparent that an increase in thermal radiation parameter leads to an increase in temperature within the boundary layer with higher impact ($Pr = 0.71$) at a smaller value of time t. Figure 9A,B brings forward the action of temperature difference C_T on temperature outlines for air and water, respectively. As temperature difference is a measure of the relative amount of internal energy within two bodies, then the high the temperature difference the high the temperature. Figure 10A,B show

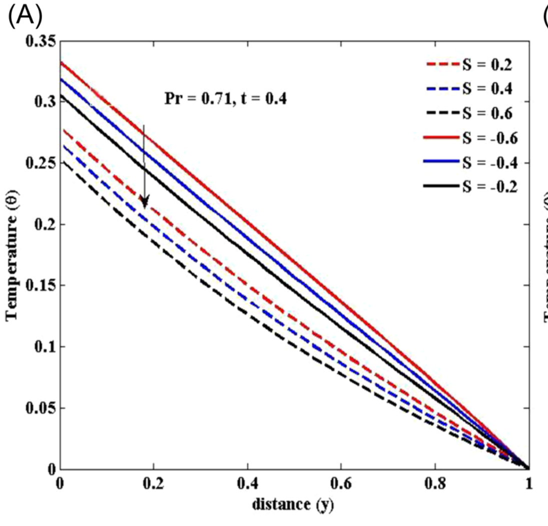

FIGURE 10 Upshot of S on temperature $\theta(y, t)$ outline

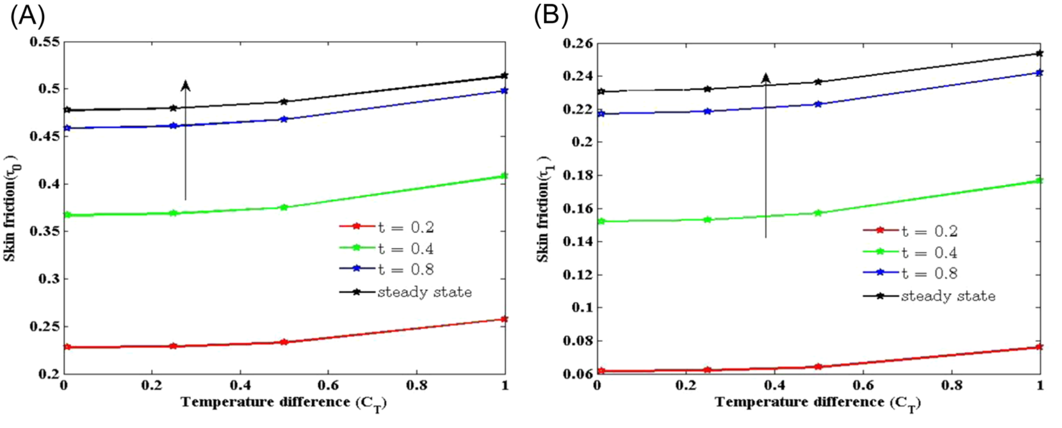

FIGURE 11 Skin friction $(\tau_{0,1})$ against C_T with changing values of time t

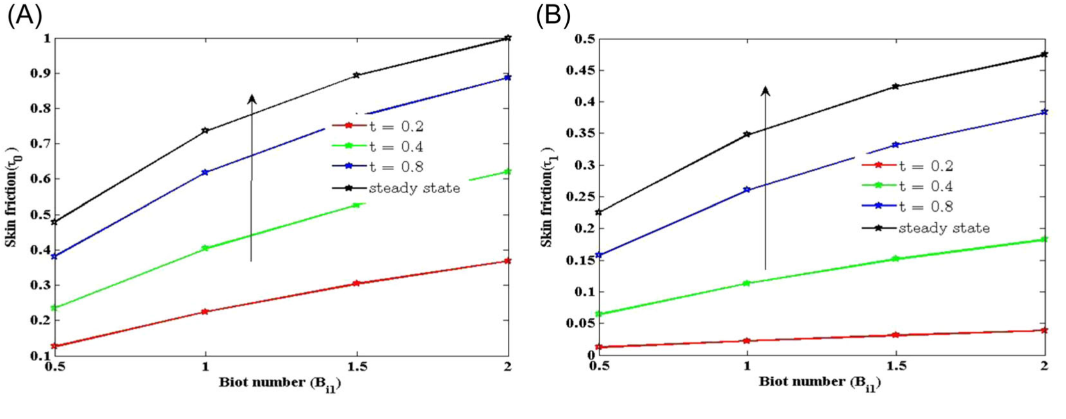

FIGURE 12 Skin friction $(\tau_{0,1})$ against B_{i1} with changing values of time t

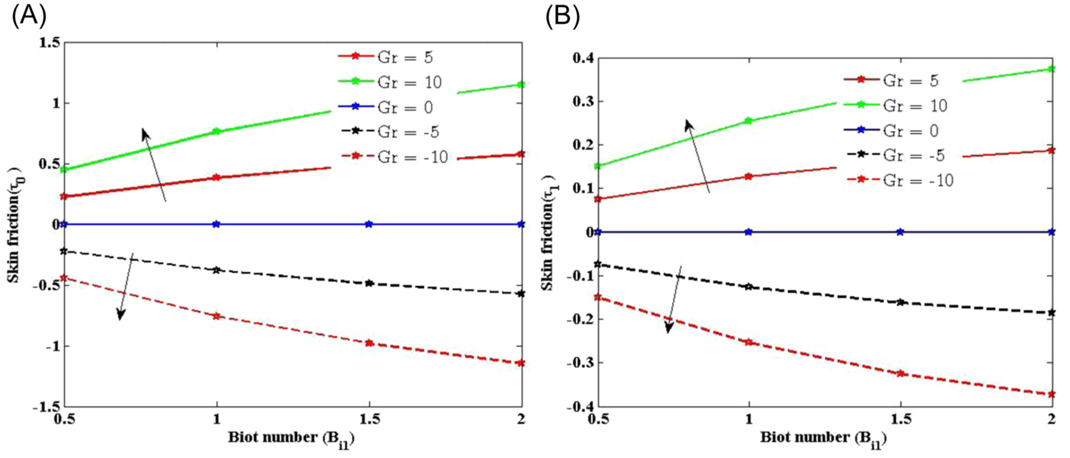

FIGURE 13 Skin friction ($\tau_{0,1}$) against B_{i1} with changing values of time t

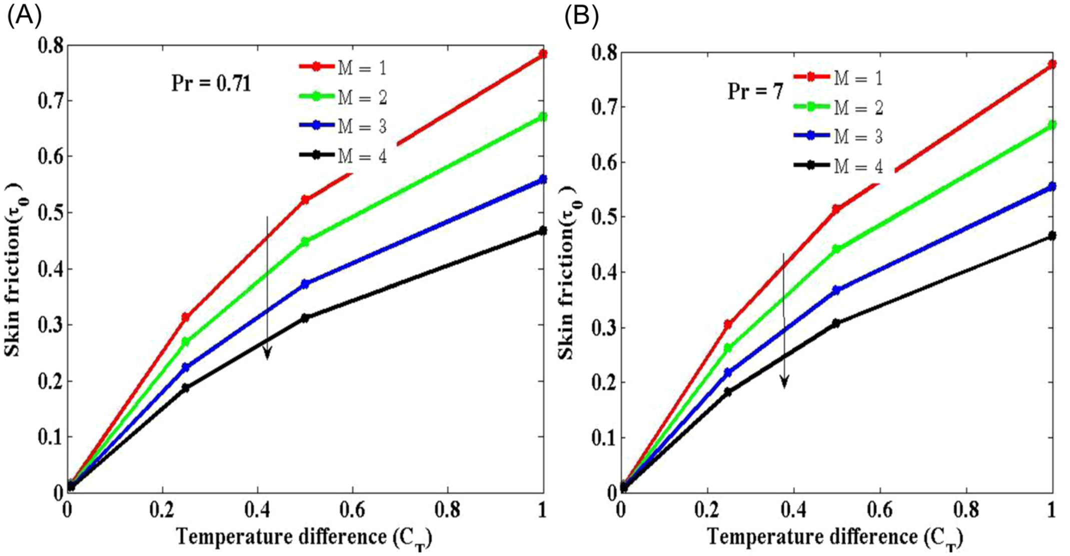

FIGURE 14 Skin friction (τ_0) against C_T with changing values of M

the influence of suction/injection parameter S on temperature outline. It is observed that temperature declines due to both suction and injection.

6.3 | Skin frictions

Figures 11–16 show the influence of C_T , B_{i1} , Gr, M, and S on skin friction at heated and cooled walls. Figure 11A,B describes the action of temperature difference C_T and time t on the skin

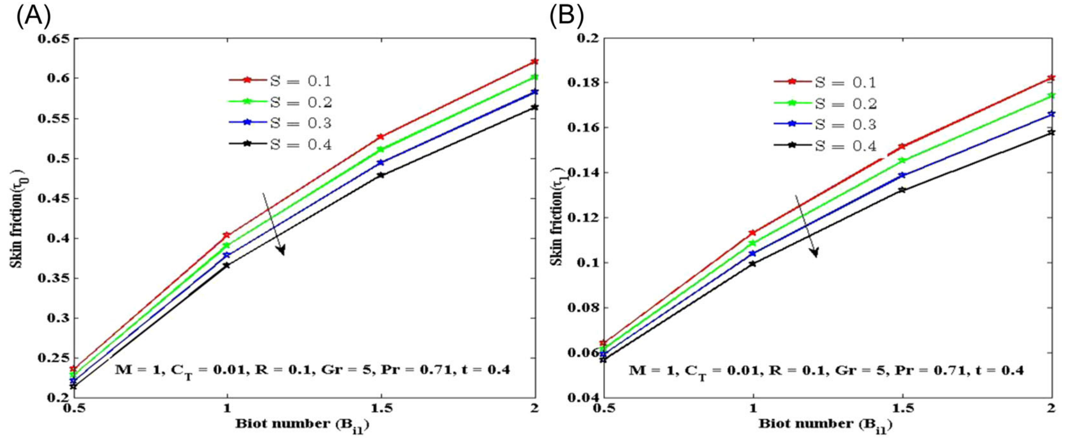

FIGURE 15 Skin friction ($\tau_{0,1}$) against B_{i1} with changing values of S ($Pr = 0.71$)

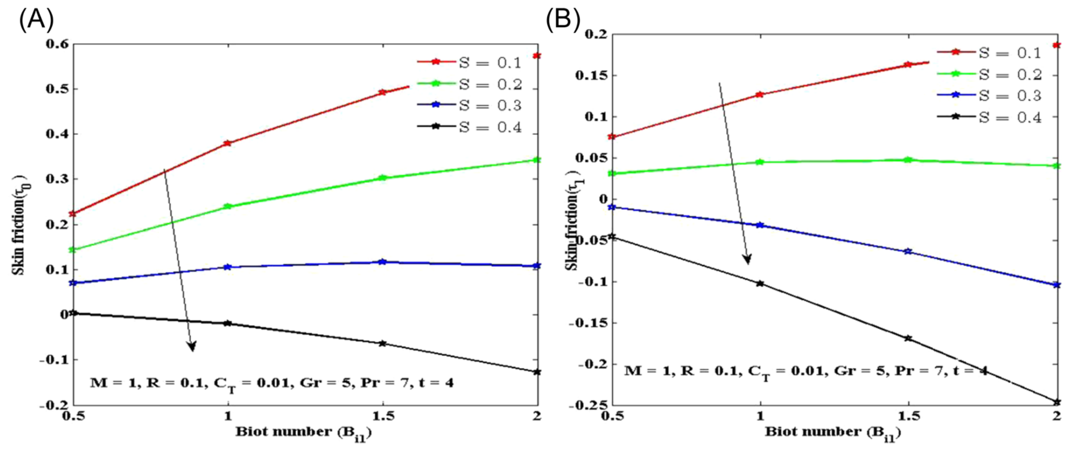

FIGURE 16 Skin friction ($\tau_{0,1}$) against B_{i1} with changing values of S ($Pr = 7.0$)

friction at the heated plate ($y = 0$) and cooled plate ($y = 1$), respectively. It is established that skin friction enhances with increasing C_T and t until it attained a steady state. It is also clear that the extent of skin friction on the convective wall ($y = 0$) is high than the values of skin friction (nonconvective wall) at $y = 1$. Figure 12A,B shows the influence of B_{i1} and time t on skin friction at $y = 0$ and $y = 1$, respectively. The result revealed that skin friction enhanced with increasing B_{i1} on both walls. Furthermore, the magnitude of skin friction at the convective plate is higher than that of the nonconvective plate at the same value of time t. Figure 13A,B shows the impact of Gr on skin frictions at $y = 0$ and $y = 1$, respectively. Changed values of Grashof ($Gr > 0$) number contributes to increasing the buoyancy force as well as decreasing the viscous forces subsequently the skin friction enhances. The presence of a convective property is attributed to the higher value of skin friction at $y = 0$. Figure 14A,B represents the profile of skin friction against C_T for chosen values of magnetic parameter M. Retarding force is dignified on skin friction when the magnetic parameter is increased and advanced with assisting values of C_T.

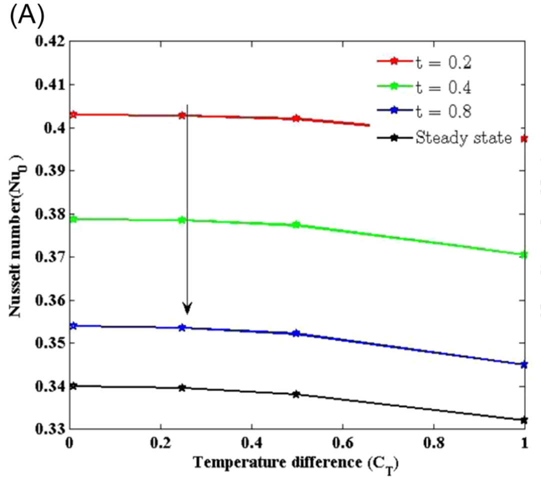

FIGURE 17 Nusselt number ($Nu_{0,1}$) against C_T with changing values of time t

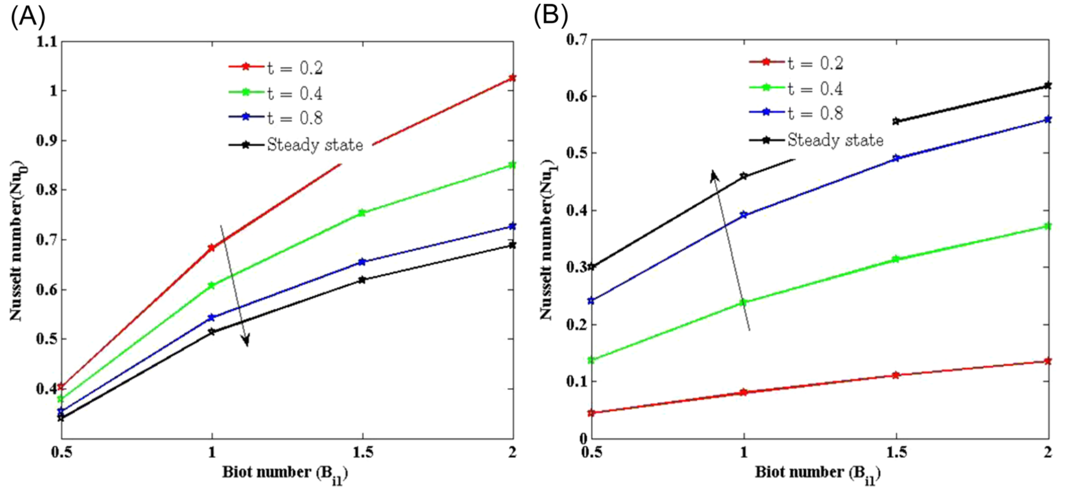

FIGURE 18 Nusselt number ($Nu_{0,1}$) against B_{i1} with changing values of time t

6.4 | Nusselt number

Figures 17–21 indicate heat transfer outlines in form of Nusselt number. Figure 17A,B shows the effects of time t and temperature difference C_T on Nusselt number at left and right plates. It shows that the Nusselt number decreases with increasing time and temperature difference at the left plate $(y = 0)$ and attains a steady-state for secure values of other monitoring parameters; whereas it enhances with increasing time and temperature difference at the right plate $(y = 1)$ and also attains steady-state. Figure 19A,B display the effect of B_{i1} and time t on Nusselt number on the left and right walls, respectively. Nusselt number declines when B_{i1}

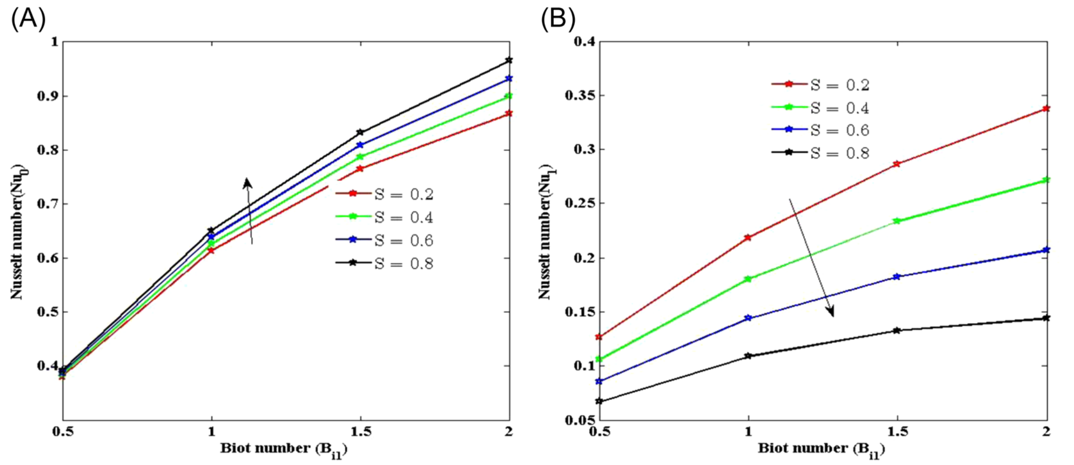

FIGURE 19 Nusselt number ($Nu_{0,1}$) against B_{i1} with changing values of S

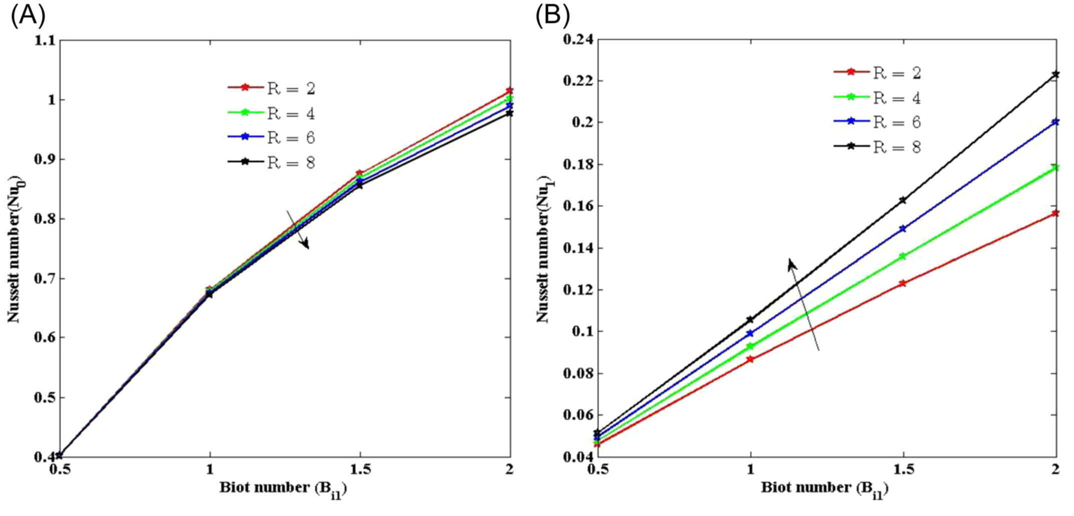

FIGURE 20 Nusselt number ($Nu_{0,1}$) against B_{i1} with changing values of R

increases at the left wall ($y = 0$) and takes the opposite trend at the right wall ($y = 1$). Figure 17A,B illustrate the Nusselt number against B_{i1} due to the influence of the suction/injection parameter ($S > 0$). Heat transfer in form of Nusselt number enhances as B_{i1} and S increase at $y = 0$ with an opposite reaction at $y = 1$. Figure 19A,B paints the impact of B_{i1} and R on the Nusselt number for the fixed value of the remaining controlling parameters. It is observed at $y = 0$, the Nusselt number declines with growing values of B_{i1} and R and later at $y = 1$. Figure 21A,B is a demonstration of the Nusselt number when B_{i1} and Pr are increased. At the convective boundary ($y = 0$) the Nusselt number tends to grow with large values of B_{i1} and Pr with converse behavior at $y = 1$.

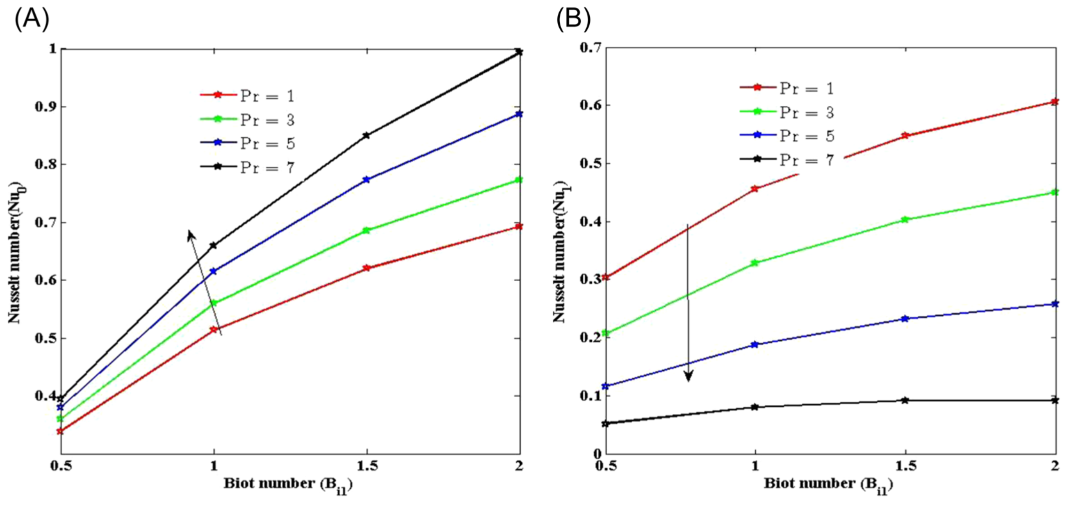

FIGURE 21 Nusselt number ($Nu_{0,1}$) against B_{i1} with changing values of Pr

7 | CONCLUSION

The steady/transient solution of MHD heat transfer flow within two porous walls aided by convective boundary conditions has been deliberated using appropriate embedded parameters. The results of the study are in form of velocity, temperature, skin friction, and Nusselt number. The finding revealed that:

i. The convective boundary condition significantly affects the velocity, temperature, skin friction, and Nusselt number.
ii. The velocity, temperature, and skin friction decay with increasing S and M while the Nusselt number upsurges with S at $y = 0$ and falls at $y = 1$.
iii. The period taken to reach a steady-state in the case of water ($Pr = 7.0$) is significantly higher in comparison with air ($Pr = 0.71$).
iv. The analytical and numerical results merged for a large value of time t and the result of the present work appears to approach that of the extended literature for a large value of Biot number.

ACKNOWLEDGMENT

I Bashiru Abdullahi wish to thank Abdu Gusau Polytechnic, Talata Mafara through Tertiary Education Trust Fund for financial support.

REFERENCES

1. Shehzad SA, Hayat T, Qasim M, Asghar S. Effects of mass transfer on MHD flow of Casson fluid with chemical reaction and suction. *Braz J Chem Eng*. 2013;30(1):187-195.
2. Uwanta IJ, Hamza MM. Effect of suction/injection on unsteady hydro magnetic convective flow of reactive viscous fluid between vertical porous plates with thermal diffusion. *Int Sch Res Notices*. 2014; 2014:980270.

3. Fenug OJ, Adigun JA, Hassan AR, Olanrewaju PO. Comment on the effects of buoyancy force and fluid injection/suction on a chemically reactive MHD flow with heat and mass transfer over a permeable surface in the presence of heat source/sink. *Int J Sci Eng Res*. 2015;6:1041-1051.
4. Jha BK, Isah BY, Uwanta IJ. Combined effect of suction/injection on MHD free-convection flow in a vertical channel with thermal radiation. *Ain Shams Eng J*. 2018;9(4):1069-1088.
5. Goyal M, Rathore KS. Effect of suction/injection, radiation and heat source/sink on MHD flow and heat transfer over an exponentially stretching sheet. *J Rajasthan Acad Phys Sci*. 2017;16(1-2):83-92.
6. Jha BK, Luqman AA, Michael OO. unsteady hydromagnetics-free convection flow with suction/injection. *J Taibah Univ Sci*. 2018;13(1):136-145. doi:10.1080/16583655.2018.1545624
7. Sasikumar J, Govindarajan A. Effects of suction and injection on MHD oscillatory convective flow in an inclined channel with oscillating wall temperatures and thermal radiation. *Int J Pure Appl Math*. 2018;119(13):289-297.
8. Hamza SEE. The effect of suction and injection on MHD flow between two porous concentric cylinders filled with porous medium. *J Adv Phys*. 2019;16:156-170.
9. Okuyade IWA, Okor T. Unsteady MHD free convective chemically reacting flow over a heated vertical plate with heat source, thermal radiation and oscillating wall temperature, concentration and suction effects. *Am J Fluid Dyn*. 2019;9(2):35-43. doi:10.5923/j.ajfd.20190902.01
10. Jitender S, Mahabaleshwar US, Bognár G. Mass transpiration in nonlinear MHD flow due to porous stretching sheet. *J Sci Rep*. 2019;9:18484.
11. Rehman S, Idrees M, Shah RA, Khan Z. Suction/injection effects on an unsteady MHD Casson thin film flow with slip and uniform thickness over a stretching sheet along variable flow properties. *Bound Value Probl*. 2019;2019:26.
12. Upreti H, Pandey AK, Kumar M. Thermophoresis and suction/injection roles on free convective MHD flow of Ag–kerosene oil nano fluid. *J Comput Des Eng*. 2020;7(3):386-396. doi:10.1093/jcde/qwaa031
13. Ferdows M, Shamshuddin MD, Zaimi K. Dissipative-radiative micropolar fluid transport in a non-Darcy porous medium with cross-diffusion effects. *CFD Lett*. 2020;12(7):70-89.
14. Dulal P, Babulal T. Influence of hall current and thermal radiation on MHD convective heat and mass transfer in a rotating porous channel with chemical reaction. *Int J Eng Math*. 2013;2013:367064.
15. Misra JC, Sinh A. Effect of thermal radiation on MHD flow of blood and heat transfer in a permeable capillary in stretching motion. *Heat Mass Transfer*. 2013;49:617-628.
16. Das K. Radiation and melting effects on MHD boundary layer flow over a moving surface. *Ain Shams Eng J*. 2014;5(4):1207-1214.
17. Kho YB, Hussanan A, Mohamed MKA, Sarif NM, Ismail Z, Salleh MZ. Thermal radiation effect on MHD flow and heat transfer analysis of Williamson nanofluid past over a stretching sheet with constant wall temperature. *J Phys Conf Ser*. 2017;890:012034.
18. Isah BY, Jha BK, Lin JE. On a Couette flow of conducting fluid. *Int J Theor Appl Math*. 2018;4(1):8-21. doi:10.11648/j.ijtam.20180401.12
19. Anil Kumar M, Dharmendar Reddy Y, Srinivasa Rao V, Shankar Goud B. Thermal radiation impact on MHD heat transfer natural convective nano fluid flow over an impulsively started vertical plate. *Case Stud Therm Eng*. 2021;24:100830.
20. Rashidi MM, Rostami B, Freidoonimehr N, Abbasbandy S. Free convective heat and mass transfer for MHD fluid flow over a permeable vertical stretching sheet in the presence of the radiation and buoyancy effects. *Ain Shams Eng J*. 2014;5(3):901-912.
21. Ibrahim W. The effect of induced magnetic field and convective boundary condition on MHD stagnation point flow and heat transfer of upper-convected Maxwell fluid in the presence of Nano particles past a stretching sheet. *Propuls Power Res*. 2016;5(2):164-175.
22. Isa SSPM, Arifin NM, Nazar R, Bachok N, Ali FM. The effect of convective boundary condition on MHD mixed convection boundary layer flow over an exponentially stretching vertical sheet. *J Phys Conf Ser*. 2017;949:012016.
23. Daniel YS, Aziz ZA, Ismail Z, Salah F. Effects of slip and convective conditions on MHD flow of nanofluid over a porous nonlinear stretching/shrinking sheet. *Aust J Mech Eng*. 2018;16:213-229.
24. Patil AB, Patil VS, Humanea PP, Shamshuddin MD, Jadhav MA. Double diffusive time-dependent MHD Prandtl nanofluid flow due to linear stretching sheet with convective boundary conditions. *Int J Model Simul*. 2022. doi:10.1080/02286203.2022.2033499

How to cite this article: Isah BY, Abdullahi B, Seini IY. On transient MHD heat transfer within a radiative porous channel due to convective boundary conditions. *Heat Transfer*. 2022;51:5140-5158. doi:10.1002/htj.22540

APPENDIX 9

$$a_{21} = \frac{B_{i1}e^{P_rS}}{B_{i1}e^{P_rS} - B_{i1} + P_rS},$$

$$a_{22} = \frac{B_{i1}}{B_{i1} - P_rS - B_{i1}e^{P_rS}},$$

$$a_{23} = \frac{a_{27}e^{x_2} - a_{28}}{e^{x_2} - e^{x_1}},$$

$$a_{24} = \frac{a_{27}e^{x_1} - a_{28}}{e^{x_1} - e^{x_2}},$$

$$a_{25} = \frac{Gra_{21}}{M^2}, a_{26} = -\frac{Gra_{22}}{P_r{}^2S^2 - P_rS^2 - M^2},$$

$$a_{27} = -a_{25} - a_{26}, a_{28} = -a_{25} - a_{26}e^{P_rS}.$$

$$C_{21} = -\frac{4}{3}C_T^3a_{22}P_r{}^2S^2 - C_T^2a_{21}a_{22}P_r{}^2S^2 - 4C_Ta_{21}{}^2a_{22}P_r{}^2S^2 - \frac{4}{3}a_{21}{}^3a_{22}P_r{}^2S^2,$$

$$C_{22} = -8C_T^2a_2{}^2P_r{}^2S^2 - 16C_Ta_{21}a_{22}{}^2P_r{}^2S^2 - 8a_{21}{}^2a_{22}{}^2P_r{}^2S^2,$$

$$C_3 = -12C_Ta_{22}{}^3P_r{}^2S^2 - 8a_{21}a_{22}{}^3P_r{}^2S^2,$$

$$C_4 = -\frac{16}{3}a_{22}{}^4P_r{}^2S^2.$$

$$f_{21} = P_rS - B_{i1}, f_{22} = (B_{i1} - 2P_rS), f_{23} = (B_{i1} - 3P_rS), f_{24} = (B_{i1} - 4P_rS),$$

$$f_{25} = f_{22}d_{24} + f_{23}d_{25} + f_{24}d_{26} - d_{23},$$

$$f_{26} = -d_{23}e^{P_rS} - d_{24}e^{2P_rS} - d_{25}e^{3P_rS} - d_{26}e^{4P_rS}.$$

$$d_{21} = \frac{f_{21}f_{26} - f_{25}e^{PrS}}{f_{21} + B_{i1}e^{PrS}},$$

$$d_{22} = \frac{f_{25} + B_{i1}f_{26}}{f_{21} + B_{i1}e^{PrS}},$$

$$d_{23} = \frac{C_{21}}{P_r S},$$

$$d_{24} = \frac{C_{22}}{2{P_r}^2 S^2},$$

$$d_{25} = \frac{C_{23}}{6{P_r}^2 S^2},$$

$$d_{26} = \frac{C_{24}}{12{P_r}^2 S^2},$$

$$x_{23} = \frac{S + \sqrt{S^2 + 4M^2}}{2}, x_{24} = \frac{S - \sqrt{S^2 + 4M^2}}{2},$$

$$G_{21} = \frac{G_{29} e^{x_4} - G_{210}}{(e^{x_{24}} - e^{x_{23}})},$$

$$G_{22} = \frac{G_{29} e^{x_{23}} - G_{210}}{(e^{x_{23}} - e^{x_{24}})},$$

$$G_{23} = \frac{Grd_{21}}{M^2},$$

$$G_{25} = \frac{-Grd_{23}}{({P_r}^2 S^2 - P_r S^2 - M^2)},$$

$$G_{24} = \frac{-Grd_{22}{P_r}^2 S^2 + Grd_{22} P_r S^2 + Grd_{22} M^2 + 2Grd_{23} P_r S - Grd_{23} S}{({P_r}^2 S^2 - P_r S^2 - M^2)^2},$$

$$G_{26} = \frac{-Grd_{24}}{(4{P_r}^2 S^2 - 2P_r S^2 - M^2)},$$

$$G_{27} = \frac{-Grd_{26}}{(9{P_r}^2 S^2 - 3P_r S^2 - M^2)},$$

$$G_{28} = \frac{-Grd_{26}}{(16{P_r}^2 S^2 - 4P_r S^2 - M^2)},$$

$$G_{29} = -(G_{23} + G_{24} + G_{27} + G_{28}),$$

$$r_1 = \frac{S\Delta t}{2\Delta y}, r_2 = \frac{\Delta t}{(\Delta y)^2}, r_3 = \frac{\Delta t}{4(\Delta y)^2},$$

$$B_l = -r_2 = B_r, B_c = 1 + 2r_2,$$

$$P = \frac{4R}{3}, z_1 = 1 + P(C_T + \theta)^3, z_2 = 4R[C_T + \theta]^2.$$